Access Published Article at https://doi.org/10.1016/j.engfailanal.2022.106975

Microstructural Defects Governing Torsional Fatigue Failure of Additively Manufactured As-Built and Heat-Treated Inconel 718

Sanna F. Siddiqui[1*] and Elise Araiza[1]

[1]Mechanical Engineering Department, Florida Polytechnic University,
4700 Research Way, Lakeland, Florida, US, 33805

***Corresponding Author:** Dr. Sanna F. Siddiqui, Assistant Professor of Mechanical Engineering, Florida Polytechnic University, (ssiddiqui@floridapoly.edu).

Abstract

Nickel-based superalloys, such as Inconel 718 (IN718), have the unique properties of high strength, oxidation, and corrosion resistance, hence necessitating their wide use in aircraft engine structural components, power-generation engines, pressure vessels, high performance automobiles, and rocket engines. Additive manufacturing (AM) of these metal superalloys is an emerging technology, which is being investigated in its capability in driving material microstructural development towards enhanced mechanical performance. With torsional fatigue as an often underlying cause for failure of components within these applications, this study investigates the microstructural defects induced through the additive manufacturing process that have driven Inconel 718 samples to failure when subjected to torsional fatigue loading conditions. As-built and heat-treated Inconel 718 torsional fatigue fracture surfaces were compared through use of a variety of material characterization techniques, to show similarities, or lack thereof, in the defects formed due to the AM process that have contributed to torsional fatigue fracture. Results from both as-built and heat-treated direct metal-laser sintered (DMLS) Inconel 718, manufactured using optimized processing parameters reveal that primary torsional fatigue cracks initiated at surface and sub-surface defects where lack of fusion regions and un-melted powder particles are apparent. Through these analyses, a correlation was made between the fracture mechanics response exhibited by each build orientation/post-processing condition and resulting torsional fatigue properties.

Keywords:

1. Mechanical Engineering
2. Fracture surfaces
3. Nickel Alloys

4. Additive Manufacturing
5. Fractography
6. Torsional Fatigue
7. Manufacturing Defect
8. Post-Processing

1. Introduction

The additive manufacturing (AM) Laser Powder-Bed Fusion (L-PBF) technologies allow for rapid prototyping of complex geometric structures and have gained much popularity due to improved efficiency in part production, yielding components with enhanced mechanical performance. Characterized by a layer-by-layer powder melting and solidification process carried out by a focused laser beam, the L-PBF additive manufacturing consists of the following processes: direct metal laser sintering (DMLS), direct metal laser melting (DMLM), selective laser melting (SLM), selective laser sintering (SLS) etc [35]. Microstructural-level defects induced through these additive manufacturing L-PBF processes (i.e., un-melted powder particles, gas pores, lack of fusion regions, porosity/voids, keyhole defects etc.) have been shown to limit the mechanical performance of additively manufactured components, specifically the fatigue performance, as they serve as localized regions of stress concentrations [1]. With the viability of the L-PBF technologies in rapidly manufacturing metal superalloy components, it becomes ever more important to improve the additive manufacturing process by limiting the presence of these microstructural-level defects, to ensure that manufactured parts meet necessary functional mechanical requirements experienced during in-service loading conditions.

Inconel 718 (IN718), a nickel-based superalloy, is used in a wide variety of applications from high performance automobiles and pressure vessels to gas turbine engine components in aircrafts, of which torsional fatigue is often an underlying cause for structural failure. A summary of select fatigue studies performed on AM Inconel 718 has been presented in Table 1. To date, there have been many studies that have explored the axial, rotating-bending, and reversed-bending fatigue performance of AM Inconel 718, along with the role of AM microstructural defects governing failure under these loading conditions [2, 4-6]. Axial high cycle fatigue (HCF) and very high cycle (V-HCF) fatigue studies reported the initiation of majority fatigue cracks from sub-surface intergranular slip bands in additively manufactured polished and machined Inconel 718 specimens [5]. Ultrasonic fatigue testing under HCF and V-HCF experiments on as-built AM Inconel 718 have reported initiation of fatigue cracks from microstructural-level defects introduced through the AM process, specifically lack of fusion (LOF) regions, gas pores and columnar grains [23]. A method has been developed for assessing additively manufactured structures for the presence of lack-of-fusion defects and pores [34]. Crystal plasticity model has also been developed to identify whether persistent slip bands or microstructural induced AM defects dominates fatigue crack initiation [22]. LOF defects occur when metal particles have not fully melted on the previous layer, leading to points of failure due to the space created, which serve as stress concentration regions [14]. Another common defect are keyhole defects, which occur when gas bubbles are trapped between the layers of melting metal. When pressure is applied, the gas bubble in the keyhole defect collapses and escapes, leading to the start of a crack that affects the overall mechanical performance [6, 13-14].

The role of AM processing parameters, specifically layer thickness, laser power, laser scan speed and build orientation were explored on the high cycle fatigue performance of as-built L-PBF Inconel 718 [20]. For those specimens developed with low laser-energy density, lack of fusion defects were evident, as compared with those specimens manufactured at high laser-energy densities in which the presence of secondary cracking and porosity were the primary sub-surface defects evident from the fracture surfaces [6, 20]. Secondary fatigue cracking and initiation of fatigue cracks at locations of un-melted powder particles and slip bands have also been reported from axial fatigue testing of AM Inconel 718 [10]. Other defects including un-melted powder particles, and regions of voids/porosity [21], have been shown to lead to failure through crack growth and rapid final fracture failure regions [5-6, 12]. Defects including high porosity enhance crack propagation, while coarse grain structure and low porosity delay crack propagation [6], in which low porosity has been shown to be reduced through the hot isostatic pressing (HIP) post-processing [15, 18]. In contrast, HIP process has also been reported to yield poor low cycle fatigue performance of AM Inconel 718 [2, 4]. AM specimens that were subjected to axial cyclic loading also showed that the integrity of the surface plays a role in the initiation of fatigue cracks [6, 9, 12, 19], nevertheless a ductile fatigue failure mode was evident by microvoid coalescence apparent in analysis of overall fracture surfaces [6, 9-10].

Only select, more recent studies have begun to present the torsional fatigue performance of AM Inconel 718 [3, 7-8]. Shear moduli and the torsional cyclic response were found for as-built and heat-treated DMLS Inconel 718 specimens manufactured along various build orientations under completely reversed angle of twist control torsional fatigue experiments [3, 7]. The impact of different heat-treatment types on the monotonic and torsional fatigue performance of L-PBF

Inconel 718 has been explored, which reported the highest torsional fatigue life for the horizontal build orientation [8].

This study is novel in that is uses material characterization techniques to identify the microstructural defects induced through the AM process, that caused torsional fatigue failure for both as built and heat-treated DMLS Inconel 718 specimens, manufactured along varying build orientations using optimized processing parameters. This study further correlates the observed torsional fracture mechanics response to shear properties reported on these samples in earlier studies [3, 7], providing a comprehensive understanding bridging processing, structure, and resulting properties with overall performance of DMLS Inconel 718 under torsional fatigue.

2. Materials and Methods

2.1 Additive Manufacturing of Inconel 718 Specimens

To investigate the impact of additively manufactured induced defects on the torsional fatigue performance of Inconel 718, specimens were manufactured using the EOS M290 direct metal laser sintering (DMLS) system with optimized additive manufacturing processing parameters as suggested by EOS. As optimized processing parameters are selected to yield a denser final product (i.e, optimal laser-energy density) for enhanced mechanical performance, it was the intent of this study to determine how the presence of any remaining additive manufacturing defects impacts torsional fatigue performance. As such, specimens were manufactured using the following processing parameters: a scanning speed of 960mm/s, laser power of 285W, layer thickness of 40μm, argon gas chamber environment, and hatch spacing of 0.11mm. As-built torsion specimens were manufactured along horizontal, diagonal, and vertical build orientations [3, 16], and their

fracture response was compared with heat-treated torsion specimens [7]. To serve as a comparison, material characterization of the torsional fatigue fracture surface of wrought (soften annealed) Inconel 718, subject to the same experimental testing conditions, was also performed. After removal of specimen support structures through electrical discharge machining (EDM), heat-treated specimens were subjected to the following heat-treatment process: solution annealing at 1950°F for 1 hour (air/argon cooling), aging at 1400°F for 10 hours (furnace cooling to 1200°F in 2 hours), hold at 1200°F for 8 hours (air/argon cooling) [7].

2.2 Mechanical Testing and Material Characterization

Completely reversed (R_ϕ =-1) room temperature angle of twist control torsional fatigue tests were performed on the as-built and heat-treated specimens specimens, at an angle of twist range of $\Delta\phi = \pm 15°$, and twisting rate of 1.654 deg/sec using the MTS EM Bionix torsion test system [3, 7]. The resulting torsional fatigue fracture response as shown in Figure 1a, and additively manufactured induced microstructural defects present within the specimens, were examined using the Zeiss Axio Vert. A1 Optical Microscope (Figure 2b), DinoLite Edge Series Digital Microscope (Figure 1b), and Hitachi SU3500 Scanning Electron Microscope (SEM) (Figure 1c) respectively. Secondary electron mode, with energy levels of 10 to 25kV was used for SEM imaging. The Buehler EcoMet 30 Manual Grinder/Polisher (Figure 2a) was used to assess the grain microstructure using the grinding/polishing procedure for nickel-based superalloys presented in [17]. The CarbiMet 240 grit abrasive disc was used during the grinding process, with a base speed of 240-300 rpm, base rotation complementary to specimen rotation. Specimen polishing was performed using the ApexHercules S rigid grinding disc with 9µm MetaDi Supreme diamond suspension for 5 min, and VexTex cloth with 3µm MetaDi Supreme diamond suspension for 5

min, using a base speed of 120-150 rpm, with base rotation complementary to specimen rotation. This was followed by use of VexTex cloth with 0.05µm Masterprep alumina suspension using a base speed of 120-150 rpm with base rotation contra to specimen rotation [17] for 2 min. Specimens were etched using the Kalling's 2 Reagent etchant solution with 35-40 wt.% Ethanol, ~2wt.% Cupric chloride, dihydrate, and 55-60wt.% of Hydrochloric acid [24]. Shear properties from [3,7] were then correlated to exhibited torsional fracture mechanics response observed and discussed in the results and discussion section.

3. Results

To correlate torsional fatigue findings reported in [3, 7] with defects at the microstructural level driving torsional fatigue failure, a variety of material characterization techniques were implored, as discussed in the experimental design section, from which the following results were found and discussed here. Torsional fatigue findings in terms of shear modulus reported in [3, 7] has been presented in Table 2, from which it is evident that heat-treatment overall was found to enhance shear moduli, *G*, with the largest shear moduli reported for the vertical and horizontal build orientations, with the lowest shear modulus reported for the diagonal build orientation [3,7]. Heat treatment was also previously reported to enhance shear stress range achieved by DMLS Inconel 718 of each build orientation [7]. Nevertheless, an analysis of grain microstructure of heat-treated sample in Figure 2d, reveals the characteristic elongated dendritic microstructure, similarly observed for as-built DMLS Inconel 718 samples [3]. This supports findings reported in [1, 25], in which heat-treatment to temperatures of 1000°C did not exhibit change in dendritic microstructure exhibited by additively manufactured Inconel 718. Melt arc pools are evident in

Figure 2c of a cross-section of the as-built AM IN718 horizontal build sample, as reported in literature.

In terms of fracture mechanics response, Figure 3 presents optical micrographic images comparing the torsional fatigue fracture response between as-built and heat-treated DMLS Inconel718, with Figure 3a for horizontal-as-built and horizontal-heat treated specimen, Figure 3b for diagonal-as-built and diagonal-heat treated, and Figure 3c for vertical-as-built and vertical-heat treated specimens respectively. Comparison between the horizontal-as-built and heat treated specimens reveals variation in the torsional fatigue fracture response with torsional fatigue crack propagation evident parallel and perpendicular to direction of build layers for a more brittle fracture response [3, 16] for the horizontal-as-built specimen. This brittle fracture response was also reported in [8] for as-built additively manufactured Inconel 718 specimens, which was suggested to be a result of the specimens not being subject to stress-relief post-processing. In contrast, the horizontal-heat treated specimen exhibits the presence of multiple fatigue cracks initiating at the surface perimeter propagating inwards within the sample. Also evident is the coalescence of 2 major fatigue cracks that initiated from the as-built specimen surface of the horizontal-heat treated specimen, leading to the final torsional fracture zone. With the as-built surface of the specimens maintained, and only variation between the specimens being subjected to the heat-treatment process, the phenomena for torsional fatigue crack initiation appears to be similar, initiating at the surface. This supports findings reported in [1, 26], in which fatigue crack initiation for the as-built specimen condition was found to proceed at the surface regardless of post-processing heat-treatment for axial fatigue studies on AM metal superalloys. Similar fatigue crack initiation sites at the surface are also evident for the diagonal as-built and heat-treated specimens as well as the vertical as-built and heat-treated specimens. Ductile failure mode appears

to dominate for the diagonal and vertical build orientations, which is explored further through SEM analysis.

SEM micrographic images were taken on samples manufactured along each build orientation (horizontal, diagonal, and vertical), and under each post-processing condition (i.e., as-built, heat-treated) to identify the microstructural defects induced through the additive manufacturing process in driving torsional fatigue failure. Figure 4 presents SEM images of surfaces of the horizontal-built samples, in the as-built condition, where torsional fatigue cracks were observed to initiate and propagate. Primary torsional fatigue cracks are observed to propagate along regions of un-melted powder particles on the rough sample surface. At higher resolution, as shown in Figure 4b, it appears that lack of fusion regions may be apparent, from which torsional fatigue cracks are commencing. This torsional fatigue crack propagation response is similar for all as-built samples, which were manufactured in the horizontal xy build plane, and supports their exhibited similar shear properties reported in [3]. Upon SEM analysis of heat-treated DMLS Inconel 718 horizontal-build fracture surface (Figure 5), multiple cracks initiating at the surface are evident, with crack sizes varying in size with smaller cracks ranging from approximately 0.10mm to 0.36mm in size to larger size cracks ranging from 0.84mm to 3.06mm in size. The larger cracks appear to coalesce and propagate to the final torsional fracture zone. A similar phenomena was reported on torsional fatigue testing of AM Ti-6Al-4V [28]. In terms of additively manufactured induced microstructural defects, regions of lack of fusion and un-melted powder particles appears near the sample surface perimeter and are suggested to have led to torsional fatigue crack initiation. The size of lack of fusion regions appears on the order of 38μm with un-melted powder particles of approximately 6 to 7μm apparent in SEM images.

SEM analysis of microstructural defects driving torsional fatigue failure of as-built diagonal-build samples is as shown in Figure 6 and 7 respectively. Compared to the horizontal-build samples, there is a significant quantity of lack of fusion regions and un-melted powder particles evident around the sample perimeter that appear to serve as sub-surface defects at which torsional fatigue crack initiation is evident. Un-melted powder particles at the surface ranged in size from approximately 18μm to 42μm. Considerable lack of fusion defects are also evident within torsional fatigue crack propagation region of fracture surface for the as-built diagonal build orientation. SEM images from heat-treated diagonal-build reveal traces of scattered un-melted powder particles on fracture surface. Due to the as-built surface, torsional fatigue crack initiation was also observed to initiate at sub-surface defects of lack of fusion regions and un-melted powder particles at the surface, regardless of the heat-treatment process. The final torsional fracture zone exhibits a dimpled rupture evident by microvoid coalescence, suggesting that ductile failure mode dominated fracture.

Overall, the diagonal-build samples exhibit considerably greater quantity of microstructural defects as compared with the horizontal-build samples. Given the importance of investigating anisotropy evident in additively manufactured metals [32-33], correlating the findings from this study to shear properties reported in [3,7,16] and highlighted in Table 2, the diagonal build orientation exhibited the least torsional fatigue performance when compared with the horizontal and vertical build samples. Table 2 presents the shear modulus obtained from the first cycle torsional fatigue data reported in [3,7,16], from which anisotropic shear modulus properties are evident with build orientation, with the diagonal build orientation yielding the lowest shear modulus. This is supported by least shear modulus reported for the diagonal build orientation

within literature as well [8]. This can be further supported by SEM micrographic images in the current study which reveal a greater quantity of additive manufacturing defects present upon analysis of the torsional fatigue fracture response.

Table 2 also expounds upon the variation in modulus of elasticity, *E*, and shear modulus, *G*, with build orientation (i.e., horizontal, diagonal, and vertical), and post-processing condition (i.e., as-built, heat-treated, and hot-isostatically pressed (HIP)) reported for L-PBF Inconel 718 across select literature. Overall, heat-treatment is found to improve modulus of elasticity and shear modulus across build orientations. It is evident from findings reported in Table 2, that while the diagonal build orientation yielded the lowest shear modulus, G, as compared with other build orientations subject to torsional loading conditions, the diagonal build orientation appears to yield a high elastic modulus, E, comparable to the horizontal build orientation, when subjected to tensile loading conditions. A review of tensile properties of AM Inconel 718 has reported that higher elastic modulus is apparent for samples subjected to "loading perpendicular to the build direction," [39], that may further support these findings.

Upon analysis of the vertical-build DMLS Inconel 718 as-built specimen (Figures 9 and 10), scarce traces of lack of fusion regions and un-melted powder particles are evident around sample perimeter, from analysis of fracture surface. Ductile fracture mode dominated failure as evident by microvoid coalescence. Analysis of heat-treated vertical-build DMLS Inconel 718 specimen reveals multiple fatigue crack initiating around surface perimeter where lack of fusion regions are evident. Due to the as-built surface, torsional fatigue crack initiation was also observed to initiate at sub-surface defects of lack of fusion regions, regardless of the applied heat-treatment process. Microvoid coalescence in final peak fracture region revealed evidence of ductile fracture response.

Of interest, are traces of un-melted powder particles and lack of fusion regions around dimpled rupture. The presence of these defects may correlate to the reported lower shear modulus reported [7] for heat-treated DMLS Inconel 718 as compared with as-built DMLS Inconel 718 [3], manufactured with the same EOS optimized additive manufacturing processing parameters.

To compare the fracture mechanics response under torsional fatigue loading conditions exhibited by additively manufactured specimens, wrought Inconel 718, with a temper rating of softened (annealed) was subjected to similar experimental conditions. It was reported to yield shear properties similar to the vertical-build as-built DMLS Inconel 718 specimen [3]. An analysis of the fracture surface in Figure 11 revealed a ductile fracture response, evident by microvoid coalescence, similar to the final fracture response exhibited by the vertical-build DMLS Inconel 718 specimens. An analysis of the surface topography revealed considerable texture especially in the region of torsional fatigue crack initiation, which was in contrast to the surface topography exhibited by the vertical build DMLS Inconel 718 samples.

4. Discussion

This study has investigated the microstructural defects induced through the AM process in driving torsional fatigue failure of as-built and heat-treated DMLS Inconel 718. It has been previously reported that to achieve ideal axial fatigue performance, a laser-energy density of 60-70J/mm^3 is recommended [6, 20] to help mitigate internal defects from impacting axial fatigue performance [6], nevertheless surface defects remain to be an eminent concern in impacting fatigue performance. In the current study, in which EOS optimized processing parameters were used to manufacture as-built and heat-treated DMLS Inconel 718 specimens for torsional fatigue testing, a laser-energy density of 67.47J/mm^3 was determined using laser power of P =285W, hatch

spacing of h = 0.11mm, laser scan speed of V = 960mm/sec, and layer thickness of t= 0.040mm from Equation (1).

$$Energy\ Density\ \left(\frac{J}{mm^3}\right) = \frac{P(W)}{V\left(\frac{mm}{sec}\right) * h(mm) * t(mm)} \quad (1)$$

Results from this study suggest that surface roughness of as-built surface, and sub-surface defects, specifically lack of fusion regions and presence of un-melted powder particles around sample perimeter are primary defects governing torsional fatigue crack initiation of as-built and heat-treated DMLS Inconel 718, manufactured using EOS optimized processing parameters. It would appear that the quantity of these defects was most pronounced for the diagonal-build specimens, as compared with the horizontal and vertical build specimens, which correlates to their deteriorating torsional fatigue performance as reported in [3,7]. Often evident from fracture surface analysis through SEM, was the presence of multiple fatigue cracks initiating around sample perimeter at or near the sample surface. This can be supported by the fact that as-built surface is determinantal to torsional fatigue performance, serving as locations for high stress concentration. As reported in [1, 27-28] on torsional fatigue studies on AM Ti-6Al-4V, shear stress is maximum furthest away from the center of the sample or at the surface.

While heat-treatment was reported to overall enhance shear modulus and shear stress range, the torsional fatigue crack initiation response near sites of these microstructural defects appears similar between as-built and heat-treated specimens. This supports findings reported in [1, 26], mentioned in the results section, in which fatigue crack initiation for the as-built specimen condition was found to proceed at the surface regardless of post-processing heat-treatment.

5. Conclusions

This study has presented novel findings on the microstructural defects introduced through the AM process in driving torsional fatigue failure of as-built and heat-treated DMLS Inconel 718 samples of horizontal, diagonal and vertical build orientations. These specimens were manufactured using optimized additive manufacturing processing parameters. Results suggest the following:

- The as-built surface roughness, and sub-surface defects including regions of lack of fusion (i.e., ~38μm) and un-melted powder particles (i.e., ~ 6 to 7μm internally, and ~18μm to 42μm at the surface) that may have led to torsional fatigue crack initiation are evident from SEM micrographic images.
- In most fracture surfaces, multiple torsional fatigue cracks were observed to initiate around surface perimeter at or near regions of these defects, with small crack sizes varying from approximately 0.10mm to 0.36mm in size, and larger crack sizes varying from approximately 0.84mm to 3.06mm in size.
- The quantity of these defects were found to be most apparent in diagonally-built specimens, which exhibited the least torsional fatigue performance as compared with the horizontal and vertical-built specimens.
- The torsional fatigue crack initiation response near sites of these AM microstructural defects appears similar between as-built and heat-treated specimens, even though heat-treatment was reported to enhance torsional fatigue performance in previous studies [3,7,16].

6. Future Work

As the additive manufacturing field advances, future work directions can also explore the material behavior of Inconel 718 under torsional fatigue loading conditions, including impacts of temperature, additive manufacturing process (i.e., Wire Arc Additive Manufacturing (WAAM) compared to Laser-Powder Bed Fusion Additive Manufacturing Process), and post-processing conditions. For example, studies have begun to explore temperature material behavior dependency on the tensile properties of WAAM IN718, including role of oxide formation, considering impacts of varying strain rate testing, and heat-treatment process [29-31], which can be extended to study torsional properties as well. It has been reported previously that while the hot isostatic pressing (HIP) technique can reduce porosity in additively manufactured IN718 components, it yields a reduced low cycle axial fatigue (LCF) performance [2, 4]. Nevertheless, the role of HIP on torsional fatigue performance and properties is yet unexplored and will be the focus of future work. Future work will also assess the role of temperature, and machined sample surface conditions on torsional fatigue performance and mitigating sub-surface defects from driving torsional fatigue failure, given that the as-built surface and sub-surface defects were most pronounced in contributing torsional fatigue fracture response observed in the current study.

Acknowledgments

This study is supported under the National Science Foundation (NSF) Grant No. (2055027), awarded to Dr. Sanna F. Siddiqui.

Data Availability

The raw/processed data required to reproduce these findings cannot be shared at this time as the data also forms part of an ongoing study.

References

[1] Sanaei, N., & Fatemi, A. (2021). Defects in additive manufactured metals and their effect on fatigue performance: a state-of-the-art review. *Progress in Materials Science*, *117*, 100724. https://doi.org/10.1016/j.pmatsci.2020.100724 .

[2] Gribbin, S., Bicknell, J., Jorgensen, L., Tsukrov, I., & Knezevic, M. (2016). Low cycle fatigue behavior of direct metal laser sintered Inconel alloy 718. *International Journal of Fatigue*, *93*, 156-167. https://doi.org/10.1016/j.ijfatigue.2016.08.019

[3] Siddiqui, S. F., & Gordon, A. P. (2020). Cyclic shear response of additively manufactured Inconel 718. *Rapid Prototyping Journal*, *26*(7), 1237-1248. https://www.emerald.com/insight/content/doi/10.1108/RPJ-09-2018-0243/full/html

[4] Aydinöz, M. E., Brenne, F., Schaper, M., Schaak, C., Tillmann, W., Nellesen, J., & Niendorf, T. (2016). On the microstructural and mechanical properties of post-treated additively manufactured Inconel 718 superalloy under quasi-static and cyclic loading. *Materials Science and Engineering: A*, *669*, 246-258. https://doi.org/10.1016/j.msea.2016.05.089

[5] Muhammad, M., Frye, P., Simsiriwong, J., Shao, S., & Shamsaei, N. (2021). An investigation into the effects of cyclic strain rate on the high cycle and very high cycle fatigue behaviors of wrought and additively manufactured Inconel 718. *International Journal of Fatigue*, *144*, 106038. https://doi.org/10.1016/j.ijfatigue.2020.106038

[6] Balasubramanian, S. S., Philpott, C., Hyder, J., Corliss, M., Tai, B., & Hung, W. N. (2020). Testing Techniques and Fatigue of Additively Manufactured Inconel 718: A Review. *International Journal of Engineering Materials and Manufacture*, *5*(4), 156-194. https://doi.org/10.26776/ijemm.05.04.2020.05

[7] Siddiqui, S. F., & Gordon, A. P. (2020, September). Torsional Fatigue of Heat-Treated Direct Metal Laser Sintered Inconel 718. In *Turbo Expo: Power for Land, Sea, and Air* (Vol. 84195, p. V008T18A006). American Society of Mechanical Engineers. Available from: https://doi.org/10.1115/GT2020-14830

[8] Sabelkin, V. P., Cobb, G. R., Doane, B. M., Kemnitz, R. A., & O'Hara, R. P. (2020). Torsional behavior of additively manufactured nickel alloy 718 under monotonic loading and low cycle fatigue. *Materials Today Communications*, *24*, 101256. https://doi.org/10.1016/j.mtcomm.2020.101256

[9] Gribbin, S., Ghorbanpour, S., Ferreri, N. C., Bicknell, J., Tsukrov, I., & Knezevic, M. (2019). Role of grain structure, grain boundaries, crystallographic texture, precipitates, and porosity on fatigue behavior of Inconel 718 at room and elevated temperatures. *Materials Characterization*, *149*, 184-197. https://doi.org/10.1016/j.matchar.2019.01.028

[10] Komarasamy, M., Shukla, S., Williams, S., Kandasamy, K., Kelly, S., & Mishra, R. S. (2019). Microstructure, fatigue, and impact toughness properties of additively manufactured nickel alloy 718. *Additive Manufacturing*, *28*, 661-675. https://doi.org/10.1016/j.addma.2019.06.009

[11] Solberg, K., & Berto, F. (2020). The effect of defects and notches in quasi-static and fatigue loading of Inconel 718 specimens produced by selective laser melting. *International Journal of Fatigue*, *137*, 105637. https://doi.org/10.1016/j.ijfatigue.2020.105637

[12] Huynh, L., Rotella, J., & Sangid, M. D. (2016). Fatigue behavior of IN718 microtrusses produced via additive manufacturing. *Materials & Design*, *105*, 278-289. https://doi.org/10.1016/j.matdes.2016.05.032

[13] King, W. E., Barth, H. D., Castillo, V. M., Gallegos, G. F., Gibbs, J. W., Hahn, D. E., ... & Rubenchik, A. M. (2014). Observation of keyhole-mode laser melting in laser powder-bed fusion additive manufacturing. *Journal of Materials Processing Technology*, *214*(12), 2915-2925. https://doi.org/10.1016/j.jmatprotec.2014.06.005

[14] Bartlett, J. L., Jarama, A., Jones, J., & Li, X. (2020). Prediction of microstructural defects in additive manufacturing from powder bed quality using digital image correlation. *Materials Science and Engineering: A*, *794*, 140002. https://doi.org/10.1016/j.msea.2020.140002Get

[15] Babamiri, B. B., Indeck, J., Demeneghi, G., Cuadra, J., & Hazeli, K. (2020). Quantification of porosity and microstructure and their effect on quasi-static and dynamic behavior of additively manufactured Inconel 718. *Additive Manufacturing*, *34*, 101380. https://doi.org/10.1016/j.addma.2020.101380

[16] Siddiqui, S.F. (2018). Characterization of anisotropic mechanical performance of as-built additively manufactured metals. Ph.D. Dissertation, University of Central Florida.

[17] BUEHLER SUM-MET The Science Behind Materials Preparation. (2007). A Guide to Materials Preparation and Analysis, BUEHLER LTD.

[18] Kaletsch, A., Qin, S., Herzog, S., & Broeckmann, C. (2021). Influence of high initial porosity introduced by laser powder bed fusion on the fatigue strength of Inconel 718 after post-processing with hot isostatic pressing. *Additive Manufacturing*, *47*, 102331. https://doi.org/10.1016/j.addma.2021.102331

[19] Balachandramurthi, A. R., Moverare, J., Dixit, N., & Pederson, R. (2018). Influence of defects and as-built surface roughness on fatigue properties of additively manufactured Alloy

718. *Materials Science and Engineering: A*, *735*, 463-474. https://doi.org/10.1016/j.msea.2018.08.072

[20] Watring, D. S., Carter, K. C., Crouse, D., Raeymaekers, B., & Spear, A. D. (2019). Mechanisms driving high-cycle fatigue life of as-built Inconel 718 processed by laser powder bed fusion. *Materials Science and Engineering: A*, *761*, 137993. https://doi.org/10.1016/j.msea.2019.06.003

[21] Sheridan, L., Gockel, J. E., & Scott-Emuakpor, O. E. (2021). Stress-defect-life interactions of fatigued additively manufactured alloy 718. *International Journal of Fatigue*, *143*, 106033. https://doi.org/10.1016/j.ijfatigue.2020.106033

[22] Dodaran, M. S., Muhammad, M., Shamsaei, N., & Shao, S. (2022). Synergistic effect of microstructure and defects on the initiation of fatigue cracks in additively manufactured Inconel 718. *International Journal of Fatigue*, *162*, 107002. https://doi.org/10.1016/j.ijfatigue.2022.107002

[23] Yang, K., Huang, Q., Wang, Q., & Chen, Q. (2020). Competing crack initiation behaviors of a laser additively manufactured nickel-based superalloy in high and very high cycle fatigue regimes. *International Journal of Fatigue*, *136*, 105580. https://doi.org/10.1016/j.ijfatigue.2020.105580

[24] ES Laboratory, LLC. Safety Data Sheet (SDS) for Kalling's 2 Reagent, Accessible from: http://nebula.wsimg.com/33cac7441c129504f0f4285b3e71e42e?AccessKeyId=628C908180FB63374807&disposition=0&alloworigin=1

[25] DebRoy T, Wei HL, Zuback JS, Mukherjee T, Elmer JW, Milewski JO, et al. (2018). Additive manufacturing of metallic components – Process, structure and properties. *Prog Mater Sci*, *92*, 112–224. https://doi.org/10.1016/j.pmatsci.2017.10.001

[26] Nezhadfar PD, Shrestha R, Phan N, & Shamsaei N. (2019). Fatigue behavior of additively manufactured 17–4 PH stainless steel: Synergistic effects of surface roughness and heat treatment. *Int J Fatigue*, *124*, 188–204. https://doi.org/10.1016/j.ijfatigue.2019.02.039

[27] Fatemi A, Molaei R, Sharifimehr S, Shamsaei N, & Phan N. (2017). Torsional fatigue behavior of wrought and additive manufactured Ti-6Al-4V by powder bed fusion including surface finish effect. *Int J Fatigue*, *99*,187–201. https://doi.org/10.1016/j.ijfatigue.2017.03.002

[28] Molaei R, & Fatemi A. (2018). Crack paths in additive manufactured Ti-6Al-4V specimens subjected to multiaxial cyclic loads. *6th International Conference on Crack Paths (CP 2018),* Verona, Italy. https://doi.org/10.1016/j.ijfatigue.2019.03.007

[29] Bhujangrao, T., Froustey, C., Iriondo, E., Veiga, F., Darnis, P., & Mata, F. G. (2020). Review of Intermediate Strain Rate Testing Devices. *Metals*, *10*(7), 894. https://doi.org/10.3390/met10070894

[30] Bhujangrao, T., Veiga, F., Suárez, A., Iriondo, E., & Mata, F. G. (2020). High-temperature mechanical properties of IN718 alloy: comparison of additive manufactured and wrought samples. *Crystals*, *10*(8), 689. https://doi.org/10.3390/cryst10080689

[31] Xu, X., Ding, J., Ganguly, S., & Williams, S. (2019). Investigation of process factors affecting mechanical properties of INCONEL 718 superalloy in wire+ arc additive manufacture process. *Journal of Materials Processing Technology*, *265*, 201-209. https://doi.org/10.1016/j.jmatprotec.2018.10.023

[32] Pérez-Ruiz, J. D., Marin, F., Martínez, S., Lamikiz, A., Urbikain, G., & de Lacalle, L. N. L. (2022). Stiffening near-net-shape functional parts of Inconel 718 LPBF considering material anisotropy and subsequent machining issues. *Mechanical Systems and Signal Processing*, *168*, 108675. https://doi.org/10.1016/j.ymssp.2021.108675

[33] Pérez-Ruiz, J. D., de Lacalle, L. N. L., Urbikain, G., Pereira, O., Martínez, S., & Bris, J. (2021). On the relationship between cutting forces and anisotropy features in the milling of LPBF Inconel 718 for near net shape parts. *International Journal of Machine Tools and Manufacture*, *170*, 103801. https://doi.org/10.1016/j.ijmachtools.2021.103801

[34] Coro, A., Macareno, L. M., Aguirrebeitia, J., & López de Lacalle, L. N. (2019). A methodology to evaluate the reliability impact of the replacement of welded components by additive manufacturing spare parts. *Metals*, *9*(9), 932. https://doi.org/10.3390/met9090932

[35] A.S.T.M. Standard. (2021). ISO/ASTM 52900:2021 Additive manufacturing-General principles-Fundamentals and vocabulary.

[36] Chlebus, E., Gruber, K., Kuźnicka, B., Kurzac, J., & Kurzynowski, T. (2015). Effect of heat treatment on the microstructure and mechanical properties of Inconel 718 processed by selective laser melting. Materials Science and Engineering: A, 639, 647-655. http://dx.doi.org/10.1016/j.msea.2015.05.035

[37] Witkin, D. B., Patel, D., Albright, T. V., Bean, G. E., & McLouth, T. (2020). Influence of surface conditions and specimen orientation on high cycle fatigue properties of Inconel 718 prepared by laser powder bed fusion. International Journal of Fatigue, 132, 105392. https://doi.org/10.1016/j.ijfatigue.2019.105392

[38] Bean, G. E., McLouth, T. D., Witkin, D. B., Sitzman, S. D., Adams, P. M., & Zaldivar, R. J. (2019). Build orientation effects on texture and mechanical properties of selective laser melting Inconel 718. Journal of Materials Engineering and Performance, 28(4), 1942-1949. https://doi.org/10.1007/s11665-019-03980-w

[39] Hosseini, E., & Popovich, V. A. (2019). A review of mechanical properties of additively manufactured Inconel 718. Additive Manufacturing, 30, 100877. https://doi.org/10.1016/j.addma.2019.100877

List of Tables

Table 1: Review of Key Literature Studies on Axial, Rotating-Bending, and Torsional Fatigue of AM Inconel 718

Study	Additive Manufacturing Process/Build Orientations	Post-Processing/AM Parameters	Experimental Design Approach	Failure Mode/Reported AM Defects
Axial/Ultrasonic Fatigue Studies				

Yang et al., *International Journal of Fatigue* (2020) **[23]**	SLM; Vertical	As-Deposited; Laser Power: 285W, Scan Speed: 960mm/s, Layer thickness: 40µm, Laser-line spacing: 0.11mm, Laser Energy Density: 67.5J/mm^3	Ultrasonic fatigue tests at 20kHz, R = -1	"• Fatigue cracks were found to initiate from microstructural defects (i.e., gas pores, lack of fusion regions and columnar grain facets) [23]."
Watring et al., *Materials Science and Engineering: A* (2019) **[20]**	3D Systems ProX DMP 320 - Laser powder bed fusion (LPBF); 0°, 60°, and 90°	As-built; Varied laser power between 115W to 465W, laser scan speed from 620mm/s to 1770mm/s and layer thickness of 30µm and 60µm, hatch spacing: 100 µm and spot size: 50 µm	Tension-tension fatigue tests with max stress of 600 MPa, R=0.1, frequency of 20 Hz	"• In HCF regime, surface roughness and volumetric laser-energy density influence fatigue life • Surface roughness causes an increase of crack initiation sites on the surface • Low laser-energy density: lack of fusion sub-surface defects dominates; High laser-energy density: keyhole pores sub-surface defect dominates along with presence of secondary cracking [20]."
Muhammad et al. *International Journal of Fatigue* (2021) **[5]**	EOS M290-Laser beam powder bed fusion (LB-PBF); Vertical and Diagonal	Heat treated according to SAE AMS2774E; Scanning Speed: 960 mm/s, Layer Thickness: 40 µm, Hatching space: 110µm, Argon Gas Chamber Environment	X-ray computed tomography for porosity analysis, Uniaxial, fully reversed force-controlled fatigue tests with R=-1, and Ultrasonic fatigue testing at 20kHz	"• 909 total identified gas-entrapped pores showing high porosity • Persistent slip bands (PSBs) as compared to volumetric defects were where fatigue cracks appeared to initiate [5]."
Komarasamy et al., *Additive Manufacturing* (2019) **[10]**	EOS M290-LPBF; Vertical and Horizontal	Heat-treated using AMS 2772, S1750SDP processes; Layer Thickness: 40 µm, Argon Gas Chamber Environment	Tensile tests; Axial force-controlled fatigue tests; Rockwell hardness tests; Charpy Impact Testing	"• Random microstructural aspects led to fatigue crack initiation (i.e., un-melted powder particle, sub-surface particle, and slip bands) • River mark type crack propagation • Cleavage/dimpled overload fracture [10]."
Solberg et al. *International Journal of Fatigue* (2020) **[11]**	Selective laser melting (SLM); Vertical	Energy Density: 60 J/mm^3, Layer Height: 50 µm	Tensile testing, Axial fatigue tests R=0 to 0.1; Notched and un-notched samples	• "Defects caused failure of notched specimens in HCF regime instead of notch root in which considerable scatter evident in failure regions [11]."

Rotating-Bending Fatigue Studies				
Gribbin et al. *Materials Characterization* (2019) **[9]**	EOS M280-Direct metal laser melting (DMLM); Diagonally, Horizontally	Hot isostatic pressing (HIP), Heat-Treated per AMS 5663, Machined; Scan Speed: 960 mm/s, Laser Power: 285 W, Laser movement: rotated 67 deg between consecutive layers, Layer thickness: 40µm	Rotating beam fatigue tests at room temp and at 500C with stress amplitudes of 200 MPa to 1200 MPa;	"• Porosity and large concentration of δ precipitates deteriorated fatigue performance at room temperature • Primary cracks initiated at largest pores near machined surface • Secondary cracks perpendicular to fracture surface developed [9]."
Torsional Fatigue Studies				
Siddiqui et al., *Rapid Prototyping Journal* (2020) **[3]**	EOS M290-DMLS; horizontal, diagonal and vertical	As-built; Layer Thickness: 40 µm, Scan Speed = 960mm/s, Laser Power = 285W, Argon Gas Chamber Environment	Torsional fatigue tests, R=-1, Angle of Twist control: $\phi = \pm 15$ deg	"• Ductile torsional fatigue response for vertical and diagonal AM and wrought specimens • Brittle torsional fatigue response for horizontal AM specimens [3]."
Sabelkin et al., *Materials Today Communications* (2020) **[8]**	Concept Laser M2 Cusing-LPBF; Horizontal (0°), Diagonal (45°), Vertical (90°),	Machined (As-Built), AMS-5662 HT and Modified HT, Varying laser power, spot size and speed for core, skin and contour sections of cylindrical samples, Layer Thickness = 40µm	Monotonic torsion tests; Fatigue torsion tests: $\phi = \pm 10°$ to $\phi = \pm 32°$	"• Primarily intergranular torsional fatigue crack initiation/propagation • Primarily ductile fracture response observed [8]."

Table 2: Tension and shear modulus at room temperature reported for AM IN718 across literature

Tensile Properties	
Study	**Results**
Chlebus et al., *Materials Science & Engineering A* (2015) **[36]**	Reported modulus of elasticity of as-built and heat-treated L-PBF Inconel 718; Horizontal (010): E =193 ± 24 GPa Horizontal (010)-heat treated: 199 ± 15 GPa Diagonal (011): E = 200 ± 23 GPa Diagonal (011)-heat treated: E = 188 ± 19 GPa Vertical (001): E = 162 ± 18 GPa Vertical (001)-heat treated: E = 163 ± 30 GPa
D. B. Witkin et al., *International Journal of Fatigue* (2020) **[37]**;	Reported modulus of elasticity of L-PBF Inconel 718 HIPed and heat-treated; Vertical: E =193.8 ± 3.4 GPa Horizontal: E = 201.7 ± 3.2 GPa Angled 45° from Z: E = 206.9 ± 1.2 GPa

G.E. Bean et al., *Journal of Materials Engineering and Performance* (2019) **[38]**	
Shear Properties	
Study	**Results**
Siddiqui et al., *Rapid Prototyping Journal* (2020) **[3]**	Reported ±shear modulus of as-built DMLS Inconel 718 with build orientation; Horizontal-as-built: G = 58.88 GPa to 60.98 GPa Diagonal-as-built: G = 46.91 GPa to 51.34 GPa Vertical-as-built: G = 70.84 GPa Wrought (softened annealed): G = 69.5 GPa
Siddiqui et al., *Proceedings of ASME Turbo Expo* (2020) **[7]**	Reported shear modulus of heat-treated DMLS Inconel 718 with build orientation; Horizontal-heat treated: G = 69.48 GPa Diagonal- heat treated: G = 55.34 GPa Vertical-heat treated: G = 66.097 GPa
Sabelkin et al., *Materials Today Communications* (2020) **[8]**	Reported shear modulus of as-built, heat-treated, and modified heat-treated L-PBF Inconel 718 with build orientation; Horizontal-as-built: G = 61 ± 1 GPa Horizontal- heat treated: G = 63 ± 1 GPa Horizontal- modified heat-treatment: G= 65 ± 1 GPa Diagonal-as-built: G = 58 ± 2 GPa Diagonal- heat treated: G = 56 ± 7 GPa Diagonal- modified heat-treatment: G = 66 ± 1 GPa Vertical-as-built: G = 80 ± 2 GPa Vertical- heat treated: G = 82 ± 3 GPa Vertical- modified heat-treatment: G = 72 ± 2 GPa

List of Figures

c.)

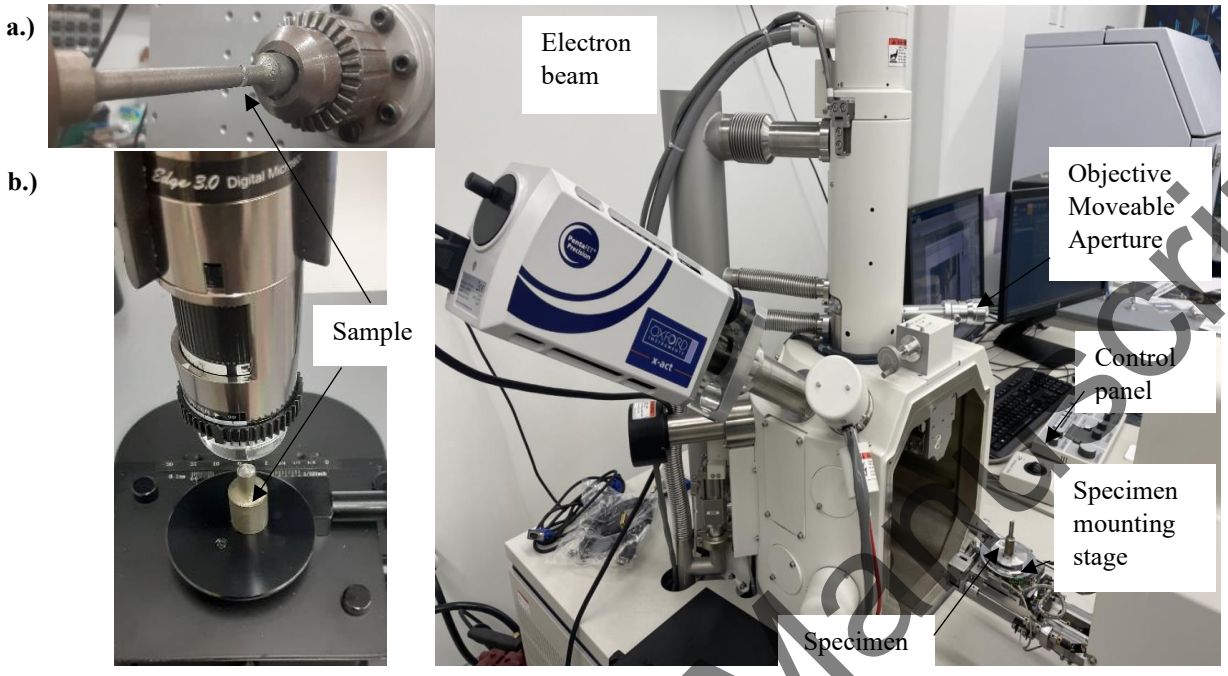

Figure 1: a) Sample fracture after torsional fatigue test; b) DinoLite Edge digital microscope (left) used to image fracture surfaces; c) Hitachi SU3500 scanning electron microscope.

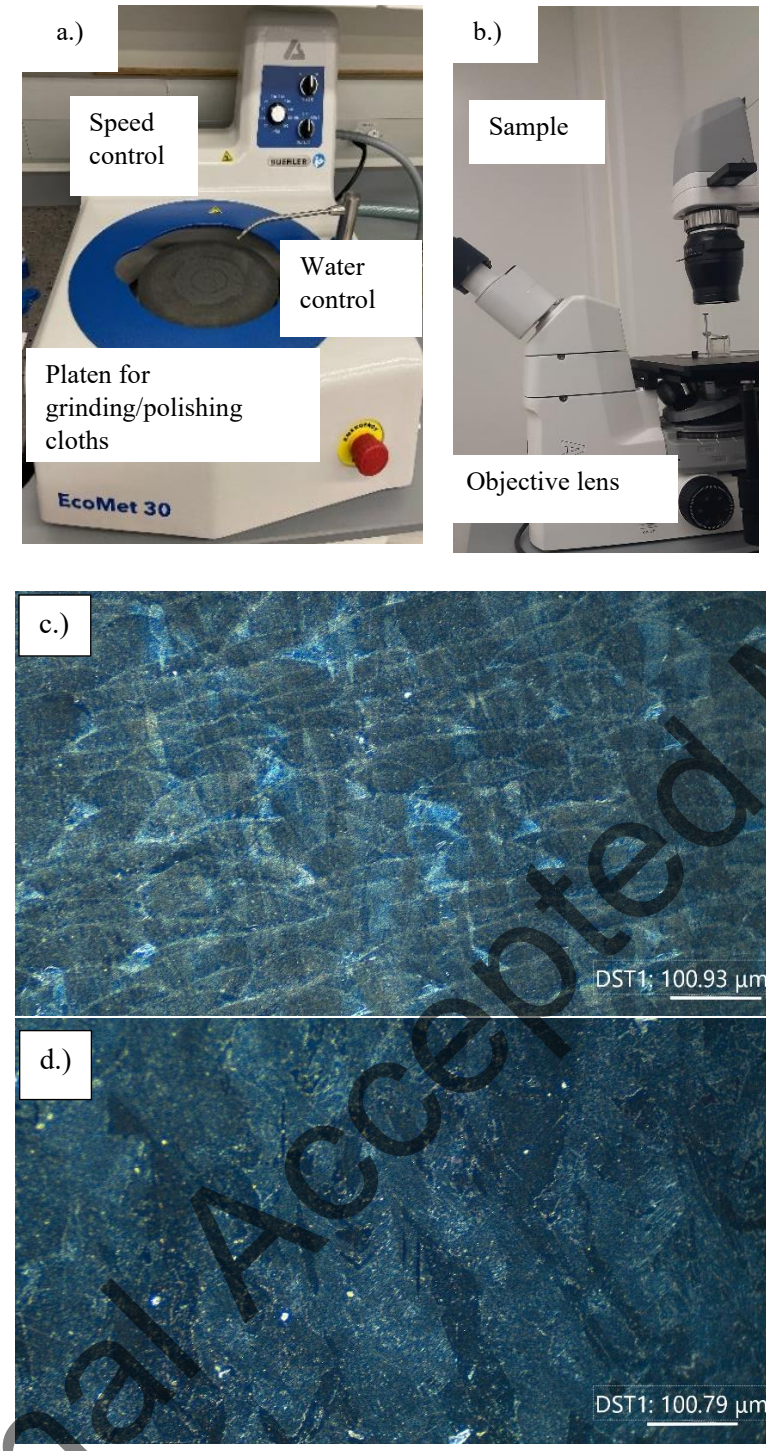

Figure 2: Equipment used for metallographic specimen preparation and analysis of grain microstructure: a.) Buehler EcoMet30 manual grinder-polisher; b.) AxioV1 optical microscope; c.) as-built Inconel 718; and d.) heat treated Inconel 718.

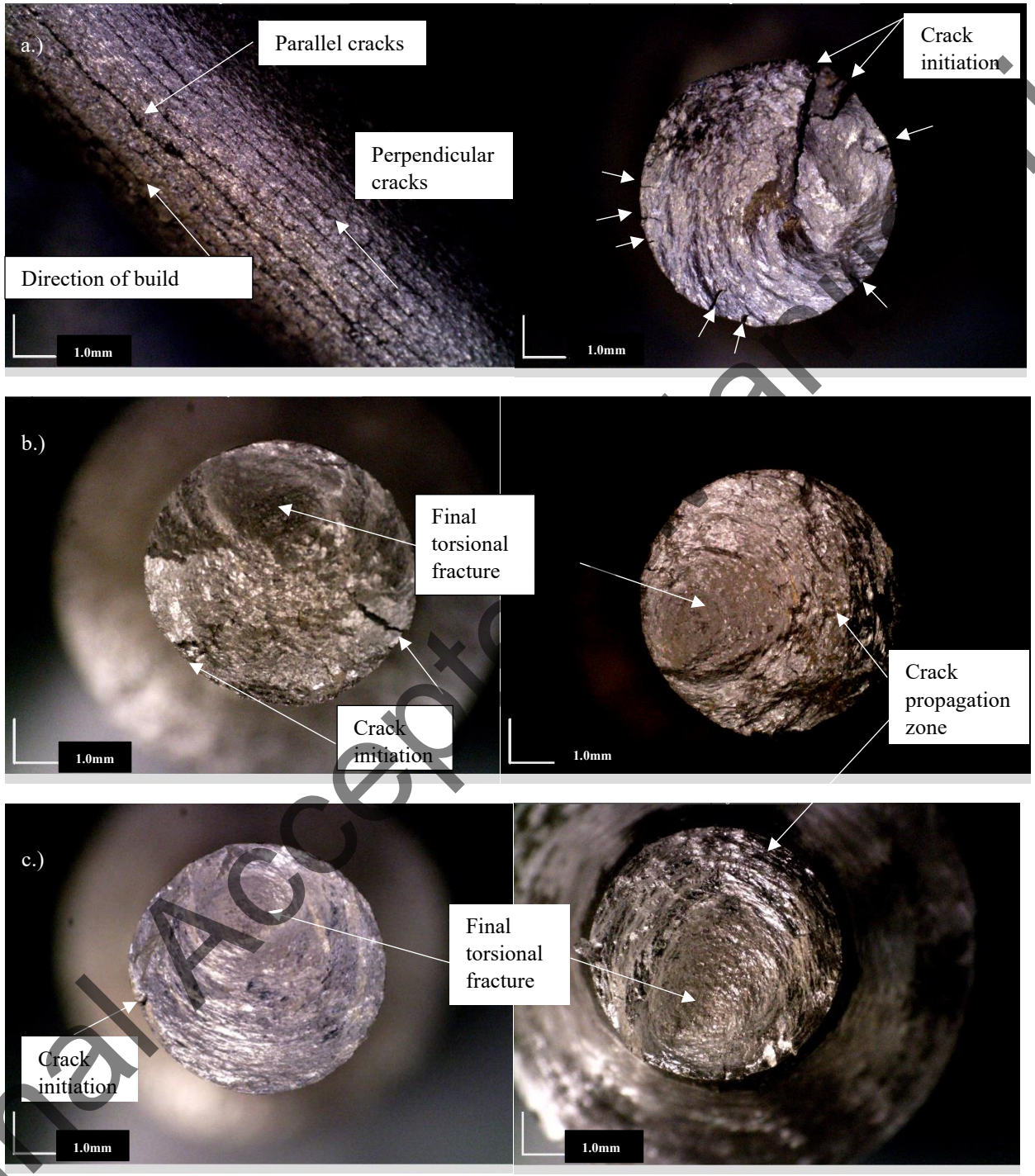

Figure 3: Optical micrographs of specimen fracture surfaces: a) horizontal-as-built & heat treated; b) diagonal- as-built & heat treated; c) vertical- as-built and heat treated.

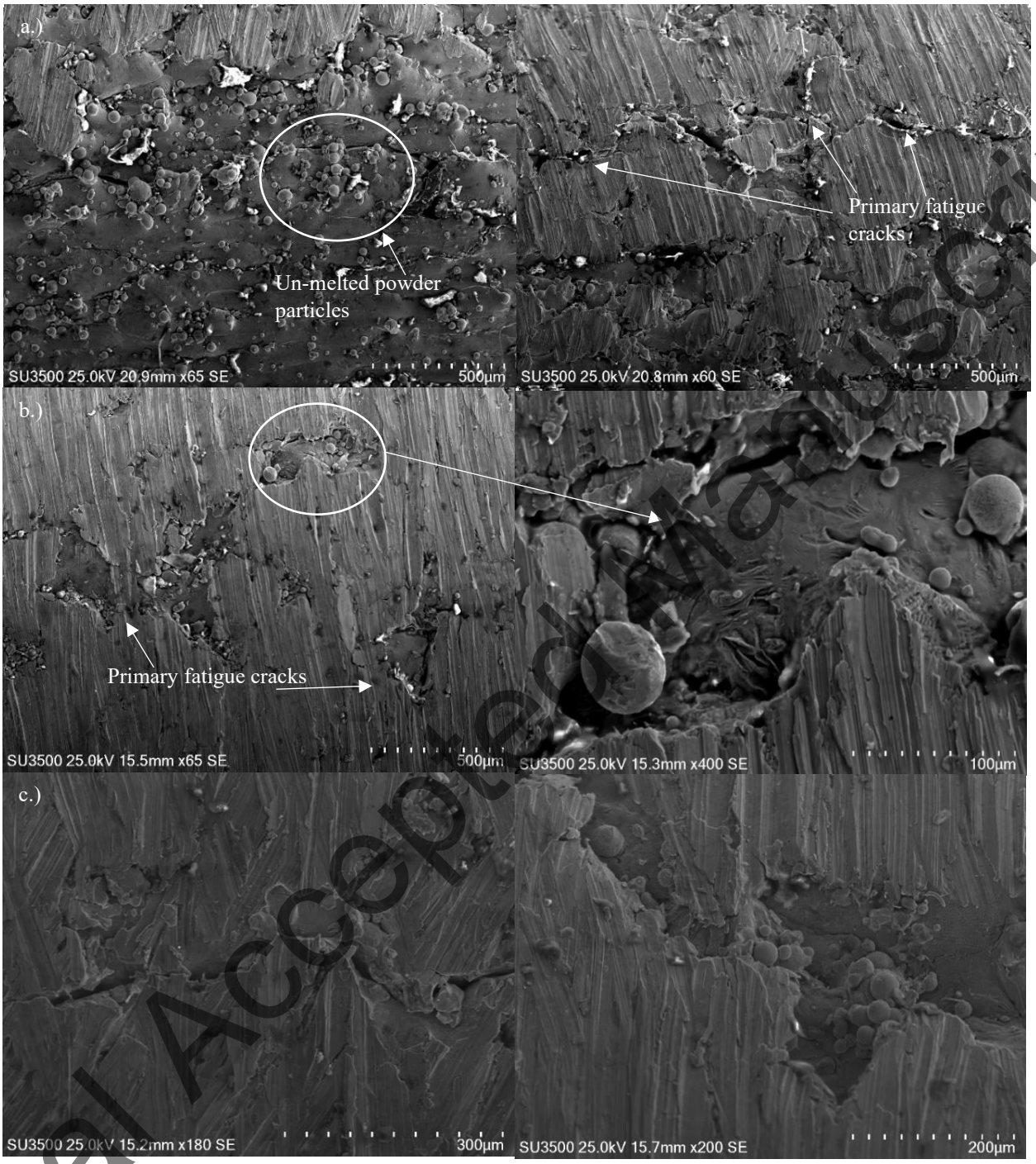

Figure 4: SEM micrographic images of L-PBF Inconel 718-horizontal-as-built specimens: a) un-melted particles within crack propagation paths on sample surface; b)-c.) primary fatigue crack paths.

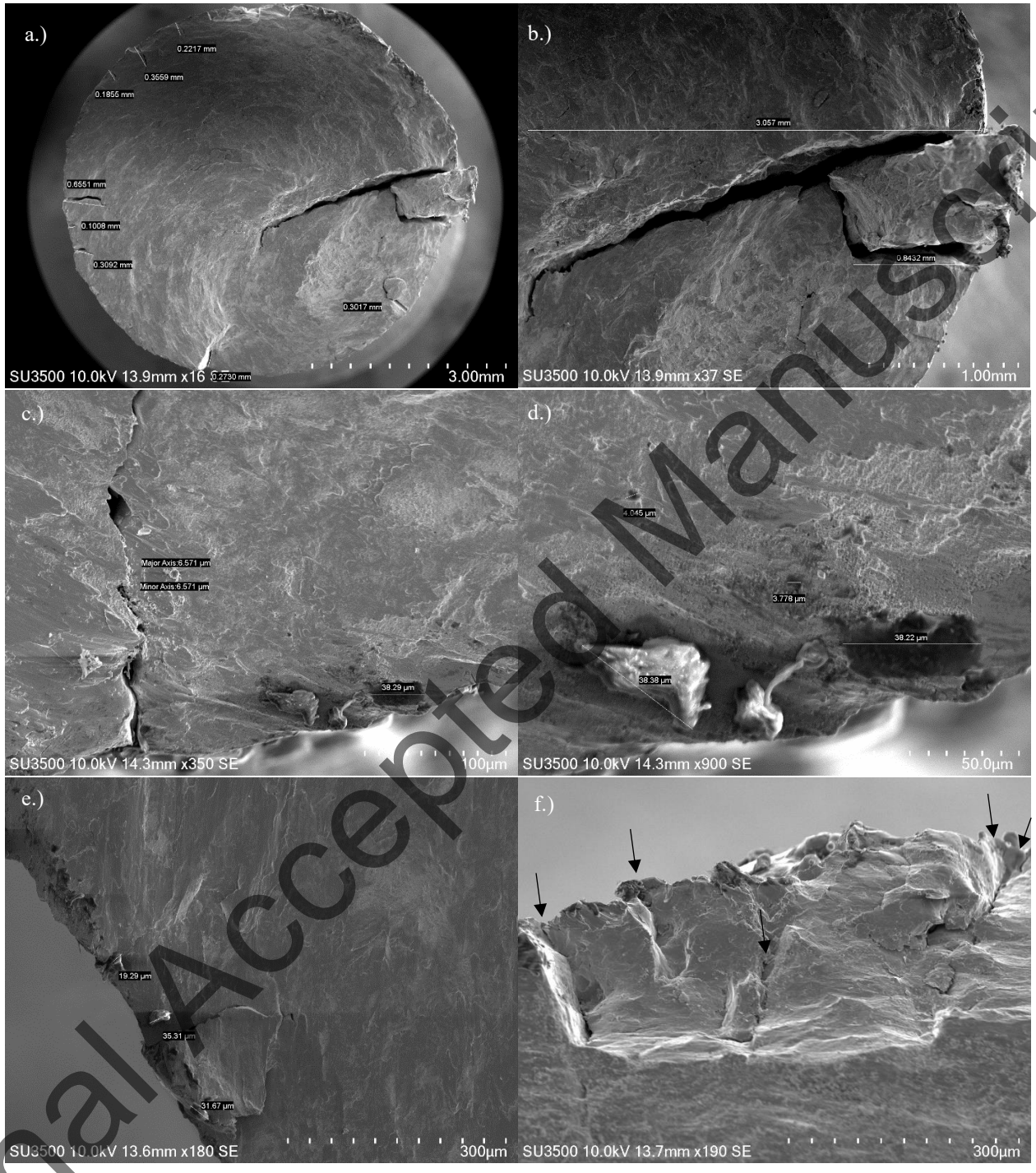

Figure 5: SEM micrographic images of L-PBF Inconel 718 horizontal-heat treated: a) overall fracture surface; b) coalescence of primary fatigue cracks initiating from surface; c), d), and e) lack of fusion regions and un-melted powder particles near sample surface resulting in multiple crack initiation sites shown in f.).

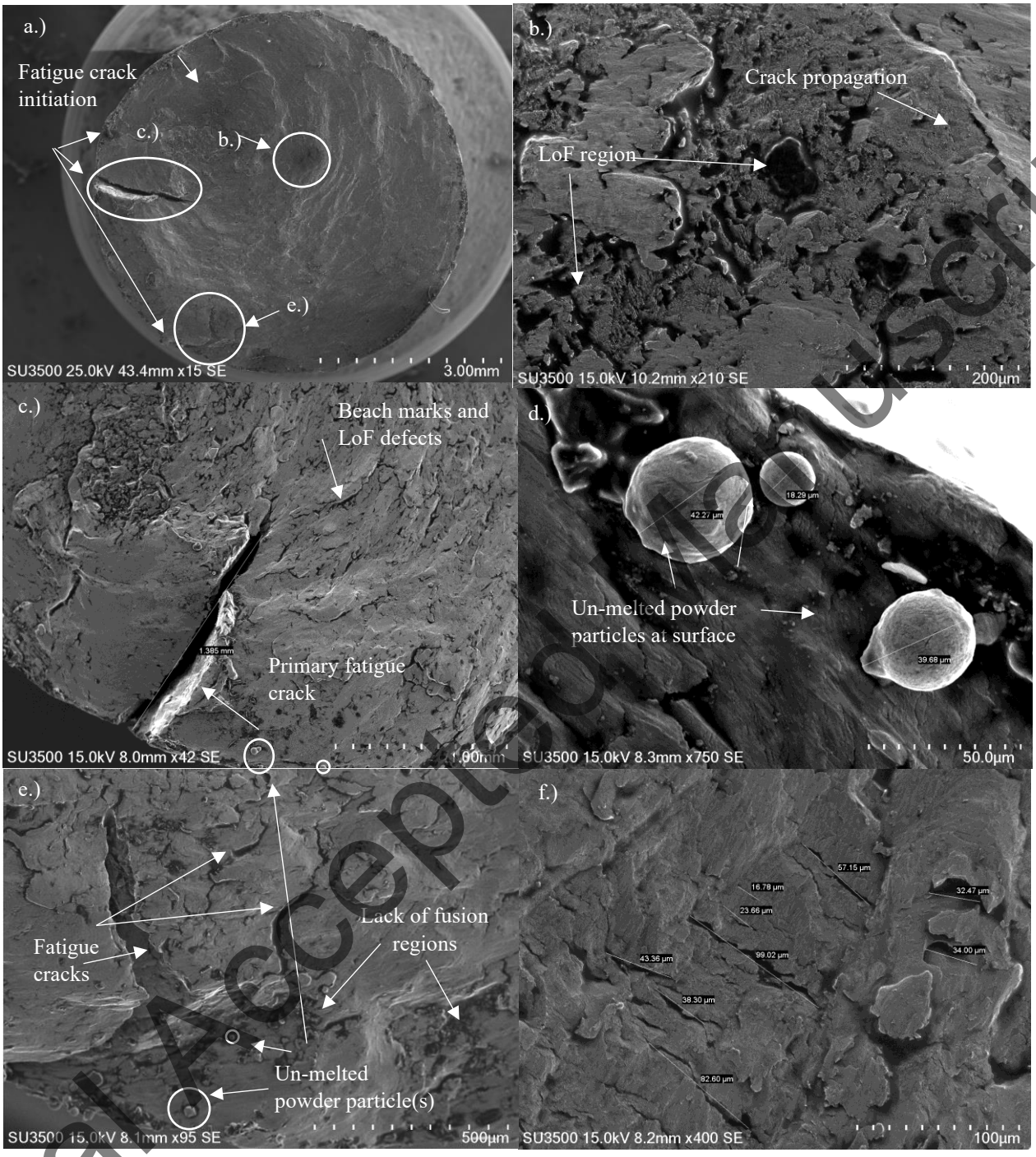

Figure 6: SEM micrographic images of L-PBF Inconel 718 diagonal as-built: a) overall fracture surface; b) visible lack of fusion area within crack propagation beach mark region; c) primary fatigue crack initiating at surface/subsurface defects; d) unfused metal particles on surface of material near edge; e.) and f.) multiple fatigue cracks initiating near lack of fusion regions.

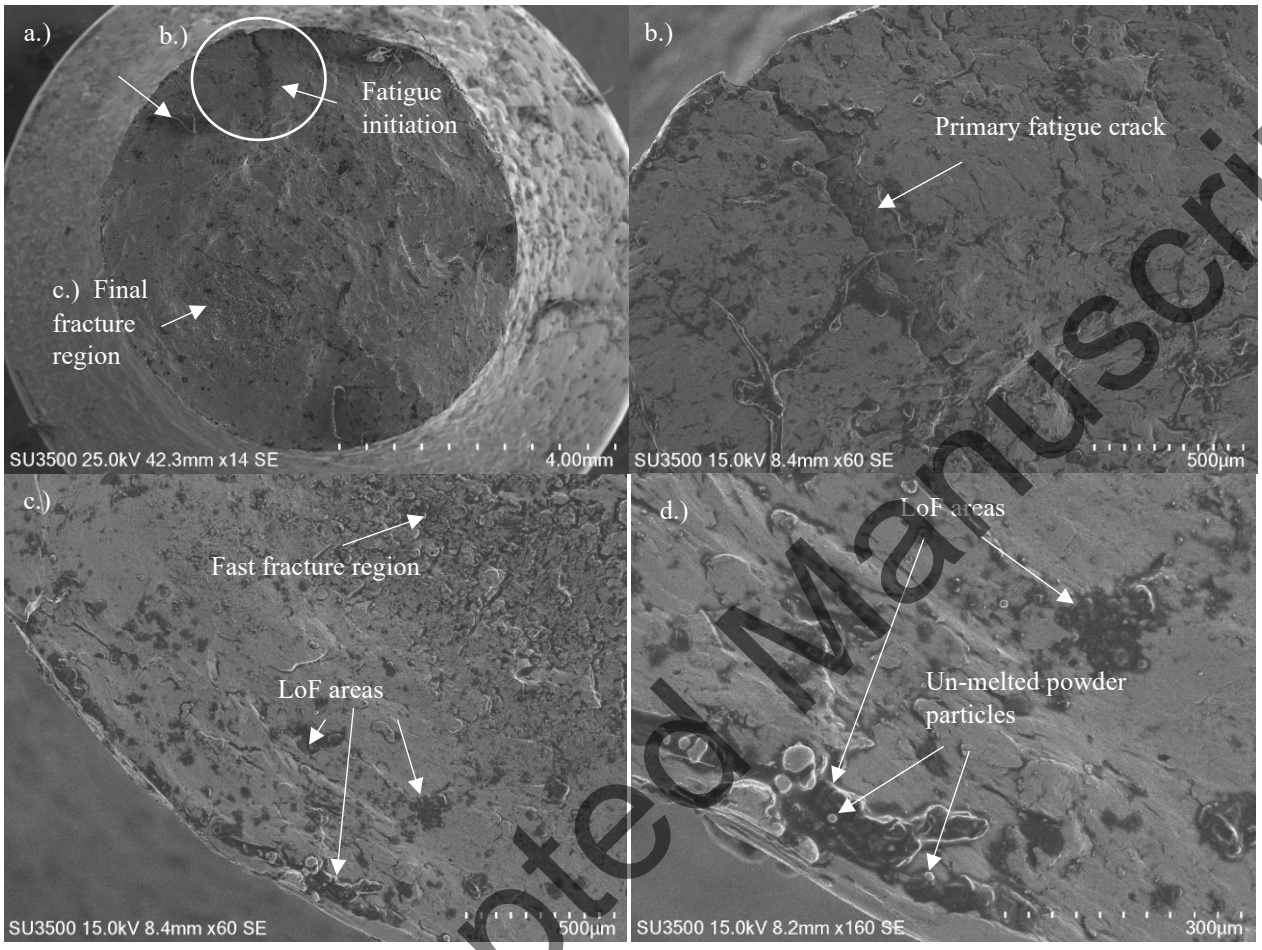

Figure 7: SEM micrographic images of L-PBF Inconel 718 diagonal as-built: a) overall fracture surface; b) primary fatigue crack initiating at surface; c) fast fracture region with lack of fusion regions evident along sample perimeter; d) high resolution of lack of fusion regions with un-melted powder particles near sample surface.

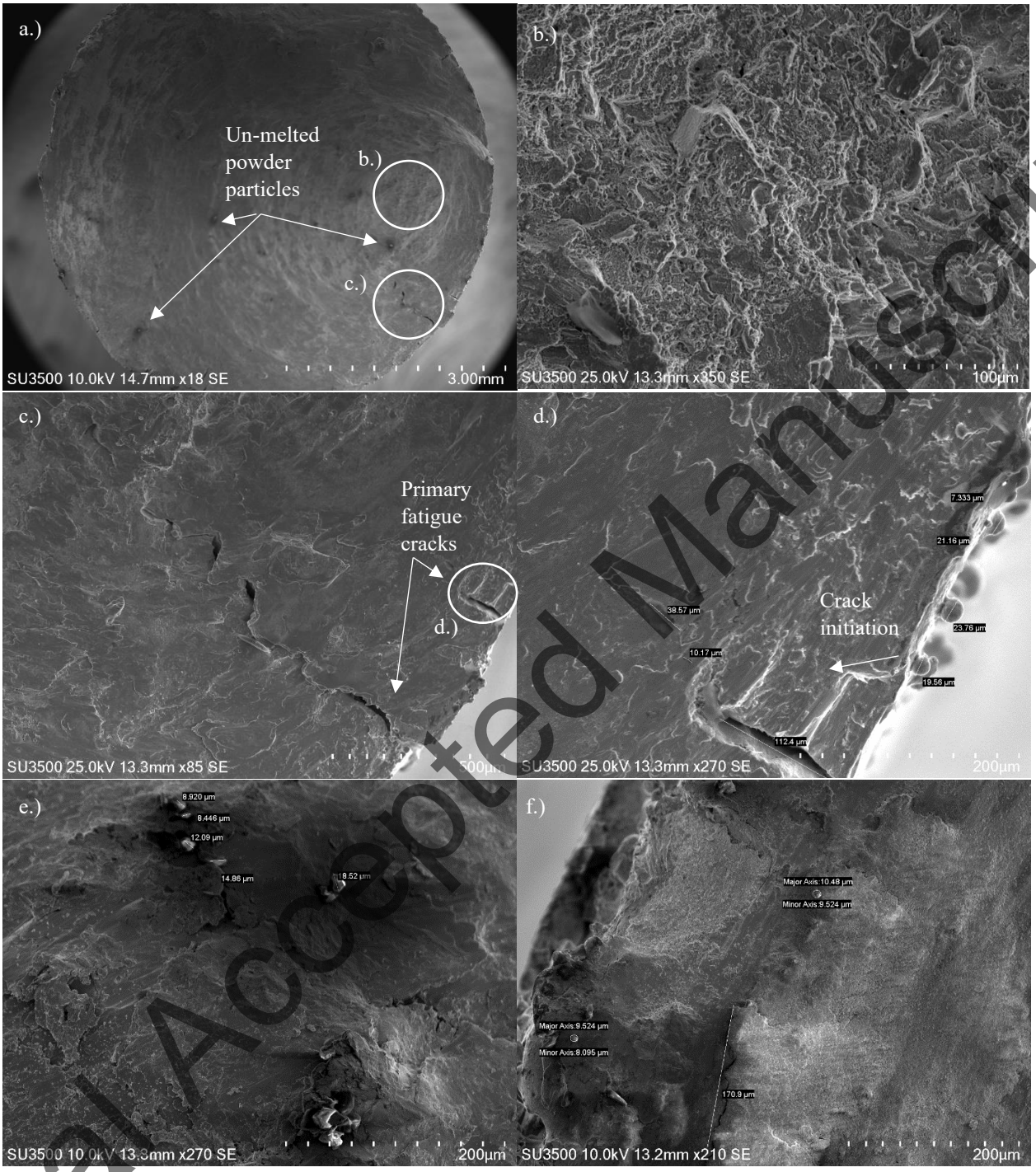

Figure 8: SEM micrographic images of L-PBF Inconel 718 diagonal-heat treated: a) overall fracture surface; b) microvoid coalescence at final torsional fracture zone; c) and d.) primary fatigue cracks initiating at surface; e.) and f.) lack of fusion regions and un-melted powder particles defects within sample.

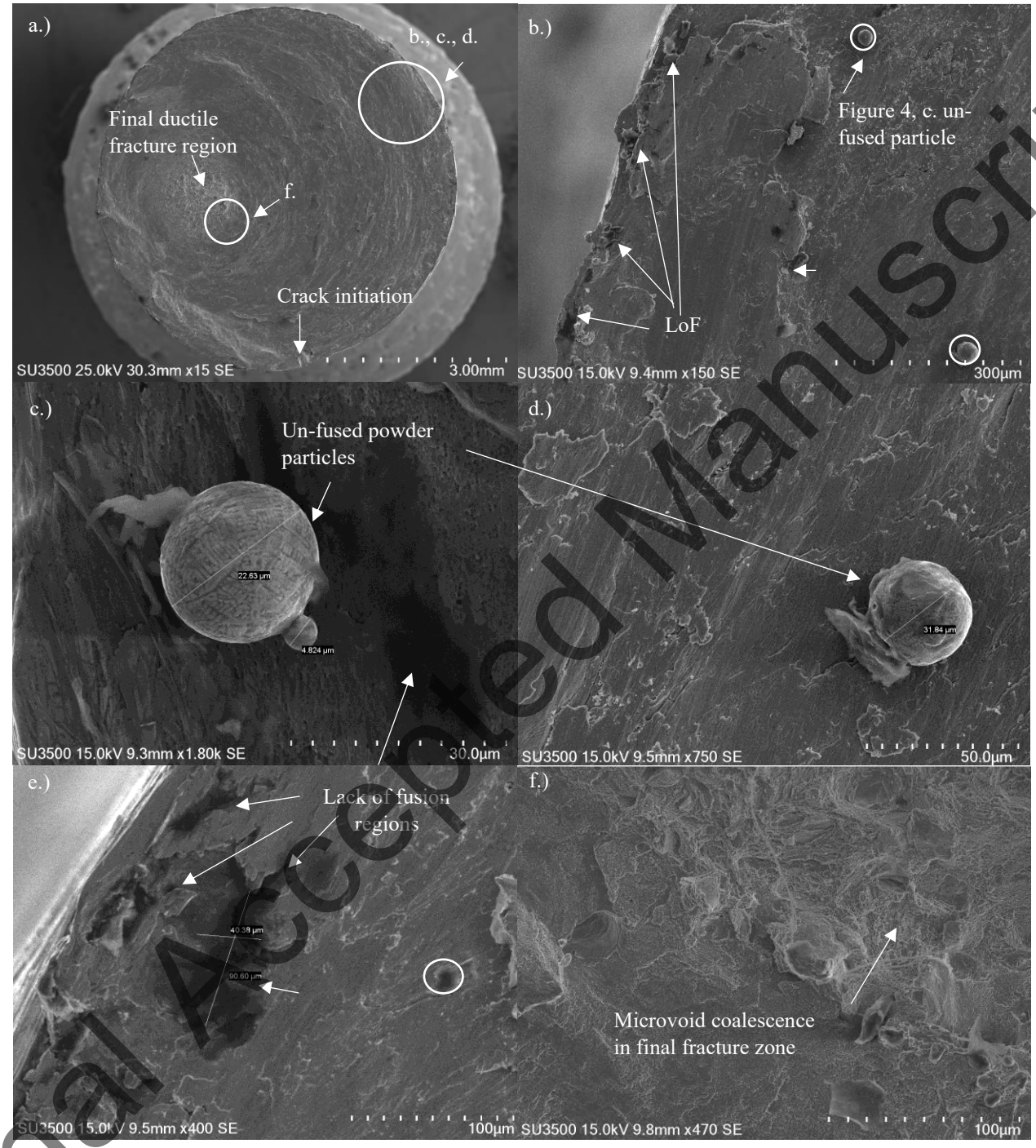

Figure 9: SEM micrographic images of L-PBF Inconel 718 vertical as-built: a) overall fracture surface; b) un-melted powder particles, balling, and lack of fusion defects evident near sample edge; c)-d) high resolution image of un-fused metal particle alongside a lack of fusion region; e) lack of fusion region near the specimen edge; f) region of microvoid coalescence leading to peak of failure.

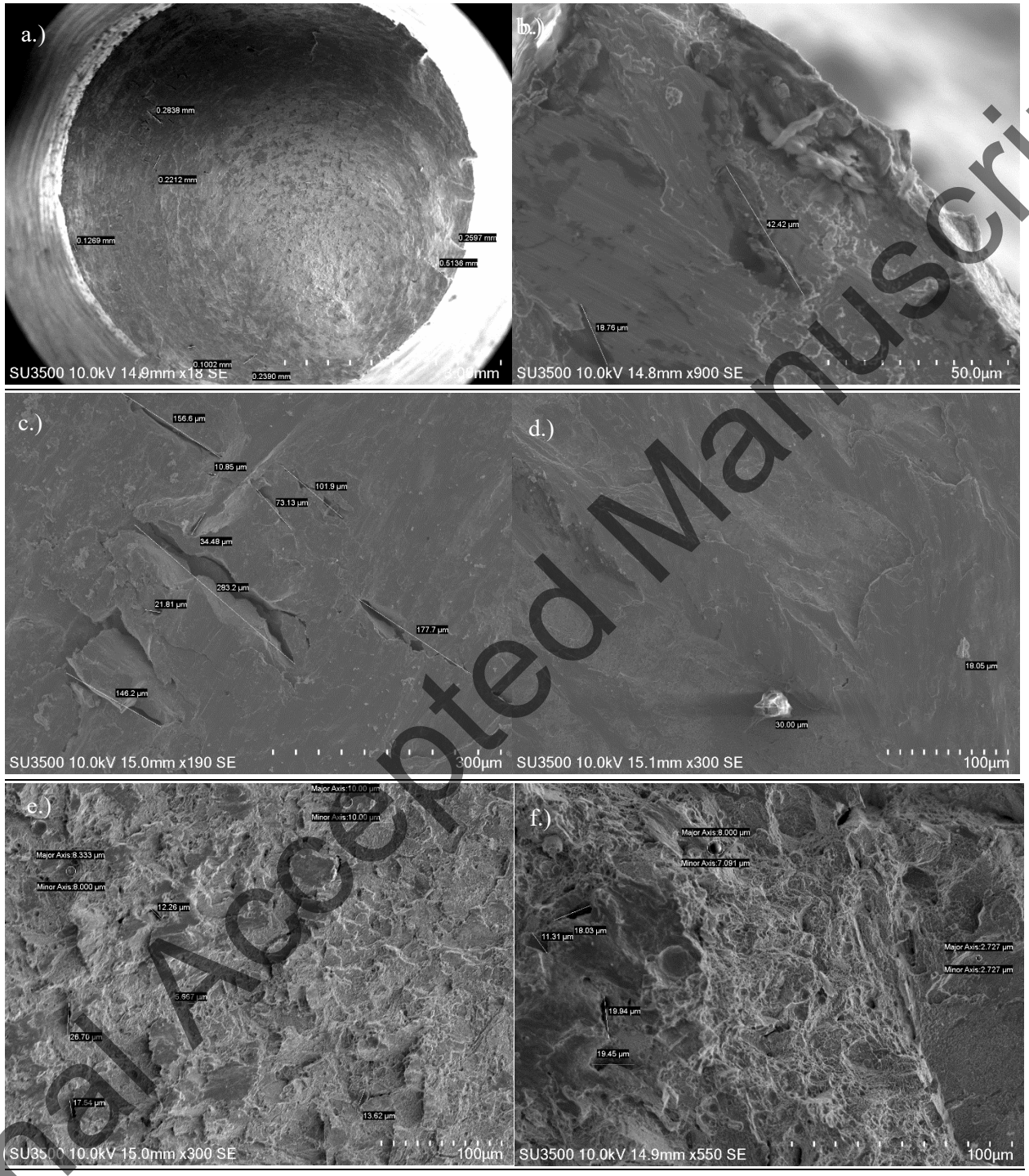

Figure 10: SEM micrographic images of L-PBF Inconel 718 vertical-heat treated: a.) overall fracture surface; b.)-f.) lack of fusion regions and un-melted powder particles apparent in fracture surface.

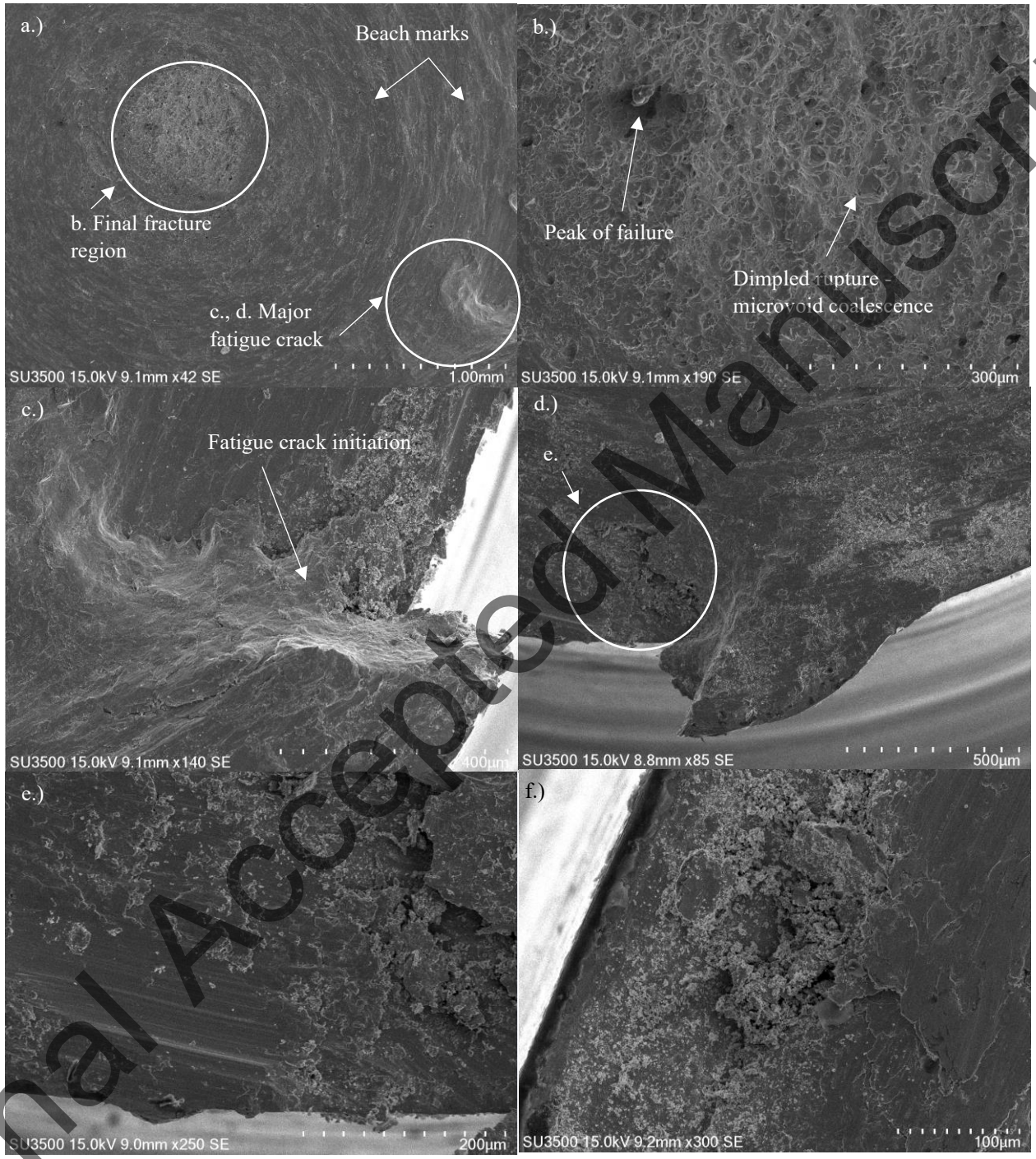

Figure 11: SEM micrographic images of Inconel 718 wrought (soften annealed): a) overall fracture surface; b) dimpled and microvoid coalescence region leading to peak of failure, c)-f.) fatigue crack initiation site.